Structural Basis for Specificity of Retroviral Proteases†

Jin Wu,‡ Jill M. Adomat,‡ Todd W. Ridky,§,|| John M. Louis,⊥,# Jonathan Leis,§ Robert W. Harrison,‡ and Irene T. Weber*,‡

Department of Microbiology and Immunology, Kimmel Cancer Center, Thomas Jefferson University, Philadelphia, Pennsylvania 19107, Department of Biochemistry, School of Medicine, Case Western Reserve University, Cleveland, Ohio 44106, and Molecular Mechanisms of Development Section, Laboratory of Cellular and Developmental Biology, National Institute of Diabetes and Digestive and Kidney Diseases, The National Institutes of Health, Bethesda, Maryland 20892

Received September 3, 1997; Revised Manuscript Received January 20, 1998

ABSTRACT: The Rous sarcoma virus (RSV) protease S9 variant has been engineered to exhibit high affinity for HIV-1 protease substrates and inhibitors in order to verify the residues deduced to be critical for the specificity differences. The variant has 9 substitutions (S38T, I42D, I44V, M73V, A100L, V104T, R105P, G106V, and S107N) of structurally equivalent residues from HIV-1 protease. Unlike the wild-type enzyme, RSV S9 protease hydrolyzes peptides representing the HIV-1 protease polyprotein cleavage sites. The crystal structure of RSV S9 protease with the inhibitor, Arg-Val-Leu-r-Phe-Glu-Ala-Nle-NH_2, a reduced peptide analogue of the HIV-1 CA-p2 cleavage site, has been refined to an R factor of 0.175 at 2.4-Å resolution. The structure shows flap residues that were not visible in the previous crystal structure of unliganded wild-type enzyme. Flap residues 64−76 are structurally similar to residues 47−59 of HIV-1 protease. However, residues 61−63 form unique loops at the base of the flaps. Mutational analysis indicates that these loop residues are essential for catalytic activity. Side chains of flap residues His 65 and Gln 63′ make hydrogen bond interactions with the inhibitor P3 amide and P4′ carbonyl oxygen, respectively. Other interactions of RSV S9 protease with the CA-p2 analogue are very similar to those observed in the crystal structure of HIV-1 protease with the same inhibitor. This is the first crystal structure of an avian retroviral protease in complex with an inhibitor, and it verifies our knowledge of the molecular basis for specificity differences between RSV and HIV-1 proteases.

Retroviral proteases are required during virus particle assembly to cleave Gag and Gag-Pol polyproteins at specific sites to produce the mature proteins that constitute an infectious virus. Crystal structures have been determined of wild-type unliganded RSV[1] protease (*1*, *2*) and of the related HIV-1 protease with and without inhibitors (reviewed in *3*). RSV protease shares 30% identical amino acid residues with HIV-1 protease and contains a conserved core structure consisting of β strands and a short α helix. While the original crystal structure of wild-type RSV protease showed many key structural features, it was missing important information for understanding substrate specificity due to disorder of the flaps. The wild-type structure was determined without an inhibitor and showed no electron density for about 10 flap residues in each subunit of the dimer. Therefore, earlier specificity studies employed a model of the flaps and peptide substrate bound to RSV protease based on crystal structures of HIV protease with various inhibitors (*4*). This model was used to predict the substrate binding residues of RSV protease in order to understand the substrate specificity. The previous studies were limited by the lack of an experimental structure for the enzyme−inhibitor complex. This paper reports the crystal structure of a mutant RSV protease where the flaps and the inhibitor are well-defined.

RSV and HIV-1 proteases possess markedly different substrate specificities, despite their structural similarities. HIV-1 protease catalyzes the cleavage, not only of its own Gag and Gag-Pol polyprotein substrates but also of the polyprotein substrates of the RSV protease (*5*). In contrast, RSV protease has a more limited range of substrates, cleaving its own polyprotein sequences but not those of HIV-1 protease. Our previous studies have identified 9 residues in the substrate-binding region of the two proteases that are critical for specificity differences (*6*). These 9 amino acids in RSV protease were substituted with structurally equivalent

† This work was supported in part by the United States Public Health Service Grants CA52047 (to J.L.), CA58166 (to I.T.W.), and AI41380 (to I.T.W. and R.W.H.) and the Intramural AIDS Targeted Anti-viral Program of the Office of the Director of the National Institutes of Health (to J.M.L.).

* To whom all correspondence should be addressed.

‡ Thomas Jefferson University.

§ Case Western Reserve University.

|| Medical Scientist Trainee supported in part by Grant GM07250 from the National Institutes of Health.

⊥ The National Institutes of Health.

Present address: Laboratory of Chemical Physics, National Institute of Diabetes and Digestive and Kidney Diseases, The National Institutes of Health, Bethesda, MD 20892.

[1] Abbreviations: HIV-1, human immunodeficiency virus type 1; RSV, Rous sarcoma virus; AMV, avian myeloblastosis virus; PR, retroviral protease; CA, retroviral capsid protein; NC, retroviral nucleocapsid protein; TF, HIV-1 transframe region; RT, reverse transcriptase; IN, retroviral integrase; SDS−PAGE, sodium dodecyl-sulfate−polyacrylamide gel electrophoresis; TFA, trifluoroacetic acid; rms, root-mean-square.

S0006-2960(97)02183-1 CCC: $15.00
Published on Web 03/13/1998

residues from HIV-1 protease. The individual mutations S38T, V104T, and S107N primarily increased the catalytic rate of the protease, while the substitutions I42D, I44V, M73V, A100L, R105P, and G106V altered the substrate specificity toward that of HIV-1 protease (*6*). These 9 mutations were combined to form an enzyme designated RSV S9 protease, which displayed kinetic parameters and specificity similar, but not identical, to those of HIV-1 protease (*7*).

In this report, we present the first crystal structure of RSV protease with visible flaps and a bound inhibitor. This structure verifies the major features of the model that was used previously (*4*) and shows additional RSV protease interactions with the inhibitor. The RSV S9 protease was crystallized with an inhibitor of HIV-1 protease, Arg-Val-Leu-r-Phe-Glu-Ala-Nle-NH_2, a reduced peptide (r) analogue of the HIV-1 CA-p2 cleavage site, with Phe substituted for Ala at P1′ and Nle substituted for Met at P3′. We show that HIV-1 protease inhibitors competitively bind to RSV S9 protease with nearly identical K_i values. Kinetic measurements confirm that the RSV S9 protease can hydrolyze additional peptides representing the natural cleavage sites of HIV-1 protease. However, the specificity is not altered completely to that of HIV-1 protease, consistent with the crystal structure showing that additional protease residues contribute to the interactions with substrates and inhibitors. The flaps of HIV-1 and RSV S9 proteases have a similar conformation, with the exception that the RSV S9 flaps contain unique three-residue loops at their bases. Mutational analysis of these loop structures indicated that they are essential for catalytic activity.

EXPERIMENTAL PROCEDURES

Construction of RSV Protease Mutants. All mutants were constructed using the megaprimer PCR method described previously (*8*), and confirmed by sequencing.

Purification of RSV S9 Protease. The histidine-tagged RSV S9 protease expressed in *Escherichia coli* was purified from the soluble fraction as described previously (*7*), resulting in a yield of 1−3 mg of active pure protease from 4 L of cells. The RSV S9 protease was also purified from the inclusion body fraction. Inclusion bodies were pelleted and solubilized in 8 M urea, 10 mM HEPES pH 8.3. Denatured protein (80 mg) was mixed with 6 mL of Ni-NTA resin (Qiagen, Chatsworth, CA) that was equilibrated in the same buffer and stirred for 1 h at room temperature. The mixture was packed into a 10-mL disposable column and washed with 8 M urea, 10 mM HEPES pH 8.3, 30 mM imidazole. The protease was eluted in the same buffer, but with 250 mM imidazole. One milliliter fractions containing the protease were pooled and renatured by dialysis against 10 mM HEPES pH 7.5, 1 mM β-mercaptoethanol for 2−3 h at 4 °C. The histidine tag was removed with 100 μg of Factor Xa (Hematological Technologies, Essex Junction, VT) and incubated overnight in 10 mM HEPES pH 8.3, 0.1 M NaCl, 1 mM $CaCl_2$. Benzamidine Sepharose 6B (Pharmacia Biotech, Uppsala, Sweden) was added to remove the Factor Xa, and the protein solution was passed again through the Ni-NTA column, which was equilibrated with 10 mM HEPES pH 8.3. The refolded and cleaved protease sample was eluted with 10 mM HEPES pH 8.3, 30 mM imidazole. One milliliter fractions of RSV S9 PR were pooled and concentrated. SDS−PAGE confirmed greater than 95% purity, and the activity was comparable to protease purified from the soluble fraction. The activity was determined by HPLC assay using the RSV NC-PR peptide substrate. A yield of at least 25 mg of pure protease was obtained from a 4-L preparation of cells.

Construction and Purification of HIV-1 Protease Mutant. An HIV-1 protease (Genbank HIVHXB2CG) clone for expression in *E. coli* was constructed with substitutions of Q7K, L33I, L63I, C67A, and C95A (Louis, unpublished, *9*). DNA sequencing identified a sixth mutation in this construct, K43E. The expressed protease was purified from inclusion bodies, as described (*10*). The mutated enzyme had proteolytic activity similar to that of the wild-type protease (Louis, unpublished).

Peptides. Peptides were synthesized by the Peptide Synthesis Facility (Kimmel Cancer Center, Thomas Jefferson University) using standard FMOC chemistry on a Millipore Model 9050 automated peptide synthesizer. The peptides were purified by reverse-phase chromatography on a Beckman System Gold HPLC with an ODS ultrasphere 10 mm × 25 cm column. Peptide concentrations were determined spectrophotometrically.

HPLC Assay for Protease Activity. Protein concentrations were determined by the Bio-Rad Protein Assay kit (Bio-Rad Laboratories) using bovine serum albumin as the standard for the calibration curve. The efficiency of refolding was determined by active site titration against stoichiometric amounts of the inhibitor, PPCV(phestatine)AMTM, as described (*6*). All protease assays were performed in 0.1 M sodium phosphate pH 5.9, 2.4 M NaCl (1 M NaCl for HIV-1 protease) at 37 °C (5). Initially, a time progression assay was performed to determine specific and relative activities. The reaction with 0.5 μM peptide in 600 μL of reaction mixture was initiated with 50 to 500 ng of protease. The reaction mixture was divided into aliquots and quenched at 5-min intervals for 1 h by adding 50 μL of 3% trifluoroacetic acid (TFA). Aliquots were injected into a Beckman HPLC ODS ultrasphere 4.6 mm × 15 cm reverse-phase column. Substrate and product peaks monitored at 210 nm were separated using a 0−100% acetonitrile gradient with 0.05% TFA. Peak areas were integrated using the Beckman System Gold program. Kinetic parameters were determined by assaying 10−2500 μM peptide at less than 20% substrate hydrolysis, usually less than 10 min (*11*). The initial rate data were fitted to a Michaelis−Menten curve using Grafit software (Erithacus). All standard errors were less than 20%. When no peptide hydrolysis was observed after 1 h, the reaction mixture was incubated for 24 h in order to test for slow proteolysis.

Fluorescent Assay for Protease Activity. Protease activity on peptide substrates related to the RSV NC-PR cleavage site (PPAVS-LAMTMRR) was measured with fluorescamine reagent as described previously (*7*).

Determination of Inhibition Constants. The K_i values for the CA-p2 analogue inhibitor were determined by Dixon analysis (*12*) for all the proteases. The K_i values for the p2-NC inhibitor were determined from IC_{50} values obtained from dose−response curves using the equation $K_i = (IC_{50} - 0.5[E])/(1 + [S]/K_m)$, where [E] and [S] are the protease and substrate concentrations (*13*), respectively.

Determination of Crystal Structure of HIV-1 Protease with a CA-p2 Analogue. Crystals were grown from a solution of 5.8 mg/mL of HIV-1 protease in 20 mM sodium acetate at pH 4.7 and 5 mM DTT with a 5-fold molar excess of inhibitor by vapor diffusion with a reservoir solution of 66 mM sodium citrate, 132 mM sodium phosphate at pH 6.2, 10 mM DTT, 10% DMSO, and 45% saturated ammonium sulfate (*14*). X-ray diffraction data were collected on an R-AXIS imaging plate detector mounted on an RU200 Rigaku rotating anode X-ray generator that was operated at 50 kV and 100 mA with a 0.5-mm collimator. Data were collected at room temperature with 2.5° oscillation frames exposed for 50 min. The distance to the detector plate was 100 mm. The unit cell dimensions were $a = 59.6$ Å, $b = 51.9$ Å, and $c = 61.7$ Å in space group $P2_1$. The data set included 20 944 independent reflections with 86.1% completeness and an *R*-merge of 8.3% at 2.0-Å resolution. The asymmetric unit of the crystals contains two dimers of HIV protease related by 180° rotation; however the two inhibitors are related by about 0° rotation. Therefore, the two dimers bind inhibitor in the opposite orientation. The structure was solved by molecular replacement using the structure of the HIV-1 protease triple mutant (Q7K, L33I, and L63I) with the CA-p2 inhibitor (*15*) as the starting model. The structure was refined to an *R* factor of 18% at 2.06-Å resolution with 184 solvent molecules and individual atomic *B* factors.

Crystallization of RSV S9 Protease with Inhibitor. RSV S9 protease (0.23 mM) was mixed with 0.3 mM CA-p2 analogue inhibitor. Using the hanging drop vapor diffusion method at room temperature, crystals appeared from a 10% saturated ammonium sulfate solution after 4 to 5 months. The crystals were hexagonal rods approximately 0.2 mm × 0.05 mm^2 in size.

X-ray Data Collection and Refinement of RSV S9 Protease. X-ray diffraction data were collected, as above, with 1.8° oscillations and 60-min exposure at 120-mm crystal-to-detector distance. The space group was determined by the symmetry and systematic absences to be either $P6_522$ with one subunit in the asymmetric unit or $P6_5$ with one dimer in the asymmetric unit. The unit cell dimensions were $a = b = 62.61$ Å and $c = 132.15$ Å. The X-ray data set consisted of 9601 independent reflections with an *R*-merge of 9.4% and was 76.8% complete at 2.4-Å resolution.

The crystal structure was solved by molecular replacement using the unliganded wild-type RSV protease crystal structure (*2*) as the starting model. The 9 mutations, the inhibitor, and flap residues 59−69 were not present in the starting model. Initially, the RSV S9 protease structure was solved in space group $P6_522$ with one subunit in the asymmetric unit. The structure was refined using XPLOR (*16*) and refitted to $2F_o - F_c$ and $F_o - F_c$ electron density maps using the program FRODO (*17*) run on a Silicon Graphics Indigo 2 workstation. Refinement was tested for one subunit in $P6_522$ and for one dimer in $P6_5$. In the higher-symmetry space group $P6_522$, the electron density map was not interpretable for the region of the inhibitor, flap residues, and mutations, although the rest of the protein was clearly visible. The inhibitor and the flap from the monomer intersected a crystallographic symmetry copy, resulting in a poorly defined electron density map in this region. The symmetry element responsible for this disorder was the 2-fold axis, which is added to $P6_5$ to generate $P6_522$. Therefore, the data were reduced in $P6_5$ and a dimer was refined in the asymmetric unit. In contrast to the substantial disorder in the higher-symmetry space group, the first electron density map for the dimer in space group $P6_5$ showed clear density for one ordered inhibitor and part of the flaps. Therefore, the refinement was continued with one dimer and one inhibitor in space group $P6_5$.

The RSV S9 protease structure had three major differences from the starting model of the wild-type RSV protease structure. There were 9 substitutions in each subunit, the CA-p2 analogue inhibitor was present, and the flap residues were ordered in the crystal structure. These differences were all located in the substrate-binding region and were introduced in separate stages during the refinement as the residues became clearly resolved in the electron density map. First, the 9 mutations were introduced in each subunit. After refinement, the inhibitor was fitted to the electron density map. When the dimer with inhibitor was refined, there was new density for the missing residues of the flaps. The tips of the flaps and water molecule clearly resembled those of HIV-1 protease. Residues 49−52 of HIV-1 protease were used to build RSV protease residues 66−69 at the tip of the flaps. Then, the flap residues 59−65 in each subunit were fitted into the $2F_o - F_c$ electron density maps during further refinement. Finally, 86 water molecules were added and the structure was refined with individual atomic *B* factors.

RESULTS

Kinetic Measurements on RSV S9 Protease. The RSV S9 protease was designed to possess the critical substrate-binding residues of HIV-1 protease. The hybrid enzyme was shown previously by the fluorescamine assay to hydrolyze peptides representing 4 natural cleavage sites of HIV-1 protease with catalytic efficiencies similar, but not identical, to those of HIV-1 protease (*7*). In this report, we have used an HPLC assay to measure kinetic parameters for RSV S9 protease hydrolysis of additional peptides that could not be measured by the fluorescamine assay due to the presence of Pro at P1′. Kinetic measurements are shown in Table 1 for hydrolysis of peptides representing three cleavage sites of HIV-1 Gag-Pol polyprotein and the RT-IN cleavage site of RSV Gag-Pol. AMV protease differs only by two amino acid residues from RSV protease and, since it is kinetically indistinguishable, has been used for comparative studies. AMV protease hydrolyzed only the RSV RT-IN peptide, while RSV S9 and HIV-1 proteases hydrolyzed all of the tested peptides. Both RSV S9 and HIV-1 proteases hydrolyzed the RSV RT-IN peptide more efficiently than did AMV protease. HIV-1 protease showed about a 2-fold increase in k_{cat} and 2-fold reduction in K_m for this substrate, compared to AMV protease. The RSV S9 protease had a greatly reduced K_m (30- to 50-fold) for this substrate, but also had a reduced catalytic rate (5- to 10-fold) compared to the other two proteases. Previously, the RSV S9 protease hydrolysis of the RSV NC-PR substrate was shown to have a 2-fold increased k_{cat} value and an 11-fold increased K_m value compared to those of AMV protease (*7*). Consistently, the RSV S9 protease has shown a 2- to 10-fold increased catalytic efficiency for hydrolysis of RSV cleavage site peptides compared to that of the wild-type enzyme and a 3-fold increase compared to that of HIV-1 protease.

Table 1: Kinetic Parameters of AMV, HIV-1, and RSV S9 Protease-Catalyzed Hydrolysis of Peptide Substrates[a]

peptide[b]	protease	K_m (μM)	k_{cat} (min^{-1})	k_{cat}/K_m (min^{-1} μM^{-1})
RSV RT-IN				
TFQAYxPLREA	AMV PR	2122	60	0.028
	HIV-1 PR	1186	111	0.094
	RSV S9 PR	37	11	0.28
HIV-1 TF−PR				
VSFNFxPQITKK	AMV PR	nd[c]		
	HIV-1 PR	562	490	0.87
	RSV S9 PR	538	15	0.03
HIV-1 PR−RT				
TLNFxPISPKK	AMV PR	nd		
	HIV-1 PR	2357	562	0.24
	RSV S9 PR	slow cleavage[d]		
HIV-1 CA-p2				
KARVLxAEAMS	AMV PR	nd		
	HIV-1 PR	101	27	0.27
	RSV S9 PR	244	10	0.04

[a] Varying concentrations of peptide substrate were incubated with different proteases, and the extent of cleavage was determined using the HPLC assay described under Experimental Procedures. [b] Site of hydrolysis is indicated by x. [c] nd denotes no detectable hydrolysis after 24-h incubation. [d] Slow cleavage indicates that products were observed only after 24-h incubation.

Table 2: Inhibition of AMV, HIV-1, and RSV S9 Proteases by Substrate-Based Analogues

HIV inhibitor	inhibition constants (nM)		
	AMV	RSV S9	HIV-1 proteases
CA-p2 analogue[a]	40 000	20	14
p2-NC analogue[b]	ni[c]	487	593

[a] Arg-Val-Leu-r-Phe-Glu-Ala-Nle-NH_2, where r indicates the reduced peptide and Nle is norleucine. The K_i values were determined by Dixon analysis (*12*) using the HPLC assay as described in Experimental Procedures with 100, 200, and 300 μM RSV NC-PR peptide substrate and 0−150 nM inhibitor. [b] Ac−Thr-Ile-Nle-r-Nle-Gln-Arg-NH_2, where Ac is acetyl. The K_i values were determined from IC_{50} values as described in Experimental Procedures. [c] No inhibition with 5 μM inhibitor.

RSV S9 protease hydrolyzed the HIV-1 TF-PR and CA-p2 peptides with k_{cat}/k_m values of about 30-fold and 7-fold, respectively, lower than those of HIV-1 protease. For hydrolysis of the TF-PR peptide, the differences were due to changes in k_{cat}, while for hydrolysis of the CA-p2 peptide, there were changes in both k_{cat} and k_m values. RSV S9 protease showed only poor hydrolysis of the HIV-1 PR-RT substrate. RSV S9 protease has been successfully engineered to hydrolyze these substrates of HIV-1 protease; however, the measured k_{cat}/k_m values are lower than those of HIV-1 protease, as observed previously (*7*).

The kinetic measurements showed that the RSV S9 protease closely reproduced the inhibitor affinity of HIV-1 protease (Table 2). Peptide analogues of the HIV-1 protease CA-p2 and p2-NC cleavage sites were tested. These two analogues were very poor inhibitors of AMV protease, while the CA-p2 and the p2-NC analogue were 20 and 500 nM inhibitors, respectively, of HIV-1 protease. The RSV S9 and HIV-1 proteases had essentially the same inhibition constants for these two inhibitors. Furthermore, the RSV S9 protease recognition of the HIV-1 CA-p2 analogue inhibitor was confirmed by the crystal structure of the complex with this inhibitor. Previously, RSV S9 protease was shown to hydrolyze the peptide substrate that is equivalent to the p2-NC inhibitor with a k_{cat}/K_m value 5-fold lower than that of HIV-1 protease (*7*). Kinetic parameters for hydrolysis of the HIV-1 CA-p2 cleavage site peptide are shown in Table 1. This peptide is longer than the CA-p2 inhibitor and has Ala instead of Phe at the P1′ position. However, the RSV S9 protease did not hydrolyze the HIV-1 protease chromogenic substrate, Lys-Ala-Arg-Nle-Phe(NO_2)-Glu-Ala-Nle-NH_2, that has P1′ Phe similar to the CA-p2 inhibitor (data not shown).

Table 3: Data Collection and Refinement Statistics for the Crystal Structures of RSV S9 and HIV-1 Proteases

	RSV S9 PR	HIV-1 PR
space group	$P6_5$	$P2_1$
unit cell dimens	$a = b = 62.61$ Å, $c = 132.15$ Å	$a = 59.61$ Å, $b = 51.94$, $c = 61.70$ Å
R-merge	9.43%	8.30%
indep reflns	9601	20 944
completeness	76.8%	86.1%
protease dimers in asym unit	1	2
inhibitor per protease dimer	1	1
resolution range for refinement	8.0−2.4 Å	8.0−2.0 Å
R factor	0.175	0.182
R free	0.293	0.281
no. of water molecules	86	184
av atomic *B* factor	18.5 Å^2	26.3 Å^2
bond length error	0.018	0.014
angle error	2.56	2.13
dihedral error	26.59	27.07
improper torsion angle	2.12	1.70

Comparison of RSV S9, Wild-Type RSV, and HIV-1 Protease Structures. Data collection and refinement statistics for the RSV S9 protease with the HIV-1 CA-p2 analogue inhibitor are summarized in Tables 3 and 4. The RSV S9 protease structure was very similar to that of the wild-type RSV protease, except that the wild-type dimer was missing flap residues 61−69 in one subunit and 59−69 in the other subunit (*2*). The root-mean-square (rms) differences were 0.63 and 0.68 Å for Cα atoms, and 0.67 and 0.72 Å for main-chain atoms, for the two superimposed subunits. Differences for the individual subunits were within the range 0.16−0.79 Å for rms differences observed between main-chain atoms in different crystal structures of the same protein (*18*, *19*). For comparison, crystal structures of HIV-1 protease with different inhibitors showed rms deviations of about 0.6 Å on Cα atoms (*3*). Comparison of the dimers of wild-type and RSV S9 proteases gave slightly larger rms differences of 0.80 Å on Cα atoms and 0.83 Å for main-chain atoms due to larger deviations of 1.5−2.5 Å in the residues 58−60, 70−71, and 70′−72′ leading to the flaps. These changes were difficult to interpret due to the absence of the flap structure for the wild-type uncomplexed enzyme and to the presence of mutations and different crystal-packing contacts in the RSV S9 protease structure. However, any conformational differences were substantially smaller than the 2−7-Å shifts in the Cα positions reported for HIV-1 protease in the presence and absence of inhibitor (*20*). The electron density maps for the CA-p2 inhibitor and the flap residues of RSV S9 protease are shown in Figure 1. All the flap residues were clearly visible, although these residues were not observed in the crystal structure of the unliganded wild-type RSV protease (*2*). The presence of ordered flaps in the RSV S9 protease crystal structure was probably due

Table 4: Resolution Dependence of Data

RSV S9 PR				HIV-1 PR			
	completeness (%)				completeness (%)		
resolution (Å)	shell	cumulative	*R*-merge (%)	resolution (Å)	shell	cumulative	*R*-merge (%)
10.00	74.0	69.0	4.1	10.00	88.6	86.9	5.5
5.00	82.7	80.6	6.0	5.00	92.4	91.7	5.9
3.00	84.2	83.4	8.1	3.00	92.0	92.4	6.7
2.79	74.6	81.7	8.6	2.75	90.2	91.9	7.1
2.40	67.8	76.8	9.4	2.50	87.0	90.7	7.5
				2.25	84.5	89.1	8.0
				2.00	76.5	86.1	8.3

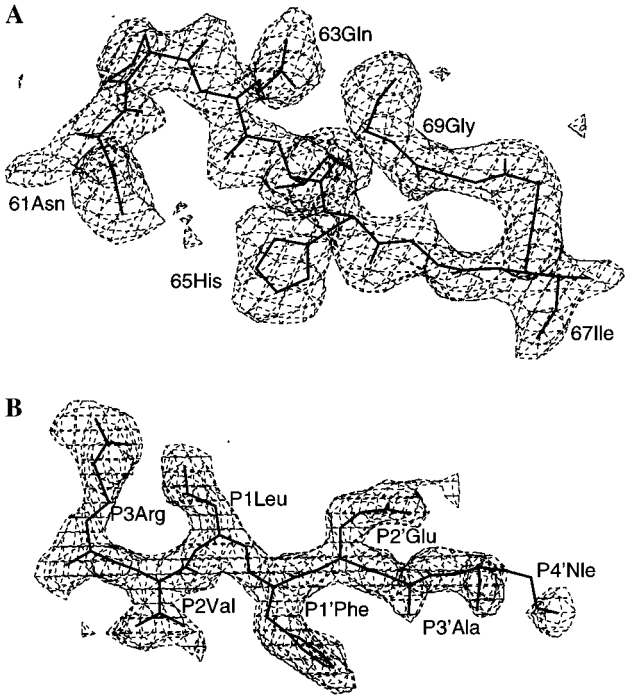

FIGURE 1: Electron density maps for RSV S9 protease showing the flap residues 60−69 (A) and the inhibitor (B). $F_o - F_c$ omit maps contoured at a level of 3σ.

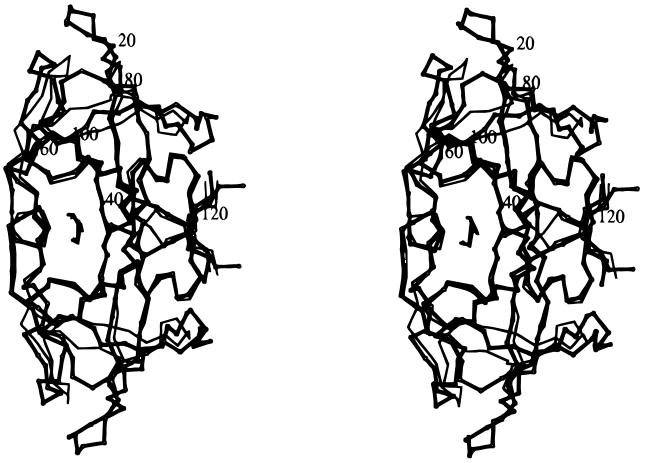

FIGURE 2: Stereoview of RSV S9 and HIV-1 proteases after superposition of the Cα atoms. The RSV S9 protease is in thick lines and the HIV-1 protease in thin lines. The Cα atoms of the two dimers are shown with the inhibitor from the RSV S9 protease structure.

to the interactions with the inhibitor, although it may have arisen from differences in the crystal lattice interactions.

For comparison, the crystal structure was determined of the HIV-1 protease with the same CA-p2 analogue inhibitor (Figure 2). The HIV-1 protease had substitutions of residues that improved the stability of the protease activity in solution in order to make it more suitable for structural studies. HIV-1 protease with mutations Q7K, L33I, and L63I was shown to be resistant to autoproteolysis and kinetically indistinguishable from wild-type enzyme (*9*), while mutations C67A and C95A eliminate the potential for protein aggregation by oxidation of cysteines without altering the enzyme activity (data not shown). The RSV S9 and HIV-1 proteases had rms deviations of 1.04 and 1.11 Å on Cα atoms and 1.15 and 1.18 Å on main-chain atoms for 86 equivalent pairs of residues in each subunit. The RSV S9 protease dimer was more similar to that of HIV-1 protease with the same inhibitor than was uncomplexed wild-type RSV protease to uncomplexed HIV-1 protease. Previous comparison of wild-type RSV and HIV-1 proteases gave rms differences of 1.45 and 1.55 Å for 86 and 88 common Cα atoms, respectively, in the two subunits (*21*). The conformation of the flaps was similar for the two proteases, especially near the tips of the flaps at the turn between HIV protease residues 50 and 51 and RSV S9 protease residues 67 and 68. The flap residues 64−76 of RSV S9 protease had an rms difference of 0.99 Å on Cα atoms compared to residues 47−59 of HIV-1 protease and a 1.05-Å rms deviation for the residues in the second subunit of the dimer. Therefore, the RSV S9 and HIV-1 protease flaps were as similar as the overall dimer structures with the CA-p2 analogue inhibitor. The regions leading to the flaps show differences in conformation for residues 48−63 of RSV S9 protease and 36−46 of HIV-1 protease.

The three crystal structures of RSV S9 protease with CA-p2 analogue, unliganded wild-type RSV protease, and HIV-1 protease with the CA-p2 inhibitor were compared for the positions of the 9 mutated residues in each subunit. The rms difference for main-chain atoms was 0.88 Å between RSV S9 and wild-type protease and 0.83 Å between RSV S9 and HIV-1 proteases, after superposition of all of the equivalent Cα atoms in the dimers. Therefore, the main-chain conformation of the RSV S9 protease mutations was more similar to the equivalent regions of HIV protease than the two structures were overall (1.21-Å rms difference on 172 equivalent Cα atoms in the dimers). Comparing RSV S9 and wild-type proteases, the largest differences were observed for residues 73′ and 104−106 in both subunits. However, these differences are probably due to the presence of inhibitor in the RSV S9 protease structure and its absence in the wild-type structure. Comparing RSV S9 and HIV proteases with the inhibitor, the largest differences were observed in the positions of the adjacent RSV protease residues 73 and 100 in both subunits, which is likely to arise from the proximity of residue 73 to the flap insertion that is

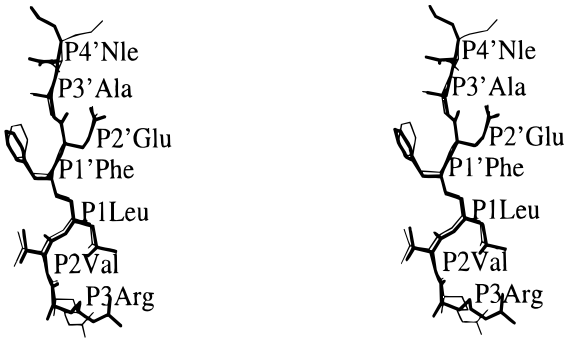

FIGURE 3: Stereoview of CA-p2 analogue inhibitors bound to RSV S9 and HIV-1 proteases. The inhibitor atoms, with residues labeled, are shown after superposition of the Cα atoms of the dimers.

absent from HIV protease. Mutations I42D, I44V, M73V, and A100L alter the S2 and S2′ subsites (*6*), while mutations R105P and G106V alter subsites S1 and S1′ (*4*). RSV protease with the single substitution S38T showed a 2-fold increase in activity over the wild-type enzyme (*7*). Since the residues D37−G39 of the catalytic triplets in the two subunits were in nearly identical positions in all three structures, the increased activity is probably due to stabilization of the catalytic residues by the additional van der Waals interactions of the Thr side chain. RSV protease with the single substitutions V104T or S107N showed increased activity compared to the wild-type enzyme, which was predicted to arise from new hydrogen bond interactions that stabilized the protease structure (*6*). The crystal structure of RSV S9 protease demonstrated that the hydroxyl side chain of Thr 104 formed hydrogen bond interactions with the carbonyl oxygen of Ala 102 in one subunit and with the carbonyl oxygen of Val 106 in the other subunit. In HIV protease, the hydroxyl of the equivalent Thr 80 interacts with the carbonyl oxygen of Val 82 in both subunits. In the wild-type RSV protease structure, the hydroxyl of Ser 107 formed two hydrogen bond interactions with the amide of Ser 46 and the carboxylate oxygen of Asp 49. In HIV-1 protease, the equivalent Asn 83 formed a similar interaction with the amide of Glu 34 and another interaction with the carbonyl oxygen of Glu 21. The crystal structure of RSV S9 protease demonstrated that the side chain of S107N formed three hydrogen bond interactions: the two observed in the wild-type enzyme and a new interaction with the carbonyl oxygen of Thr 33, similar to that in HIV-1 protease. These interactions would be expected to stabilize the conformation of residues 104−107 in RSV S9 protease and 80−83 in HIV protease that are critical for recognition of substrate positions P1 and P1′.

The two dimers of HIV protease in the asymmetric unit of the crystal structure bind the CA-p2 analogue in opposite directions, since the two subunits in a dimer can be distinguished by the intersubunit hydrogen bond between Ile 50 C═O and NH of Gly 51′. In one dimer, the amino-terminal residues P3−P1 of the inhibitor are bound in the first subunit, while the P1′−P4′ residues are bound in the second subunit. In the other dimer, the inhibitor P3−P1 residues are in the second subunit and the P1′−P4′ residues in the first subunit. The inhibitor in the RSV S9 protease was compared with the inhibitor that was bound in the same direction in HIV protease (Figure 3). The two inhibitors had almost the same conformation in the dimers of RSV S9

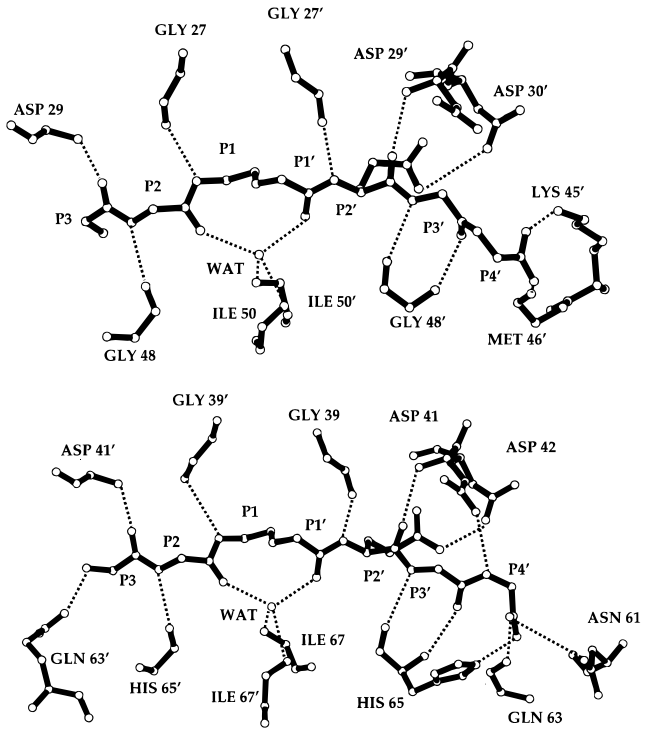

FIGURE 4: Interactions of RSV S9 and HIV-1 proteases with the inhibitor. HIV protease is shown in the upper panel and the RSV S9 protease in the lower panel. The inhibitor is an analogue of the HIV-1 CA-p2 cleavage site, Arg-Val-Leu-r-Phe-Glu-Ala-Nle-NH_2, where r is the reduced peptide bond, $-CH_2-NH-$, and Nle is norleucine. Only main-chain atoms of the inhibitor are shown, except for the side chain of P2′ Glu. Hydrogen bond interactions are indicated by dotted lines.

and HIV-1 proteases, except for the distal P3 and P4′ side chains. Residues at P2, P1, P2′, and P3′ were essentially in identical conformations. The inhibitor side chains of P1′ Phe in the two proteases were related by a small rotation, and there was a corresponding shift in the positions of the side chains of residues Val 106/82, Arg 10/8, and Ile 108/84 in RSV S9/HIV-1 proteases. The distal side chains of P3 Arg and P4′ Nle of the inhibitor were in different conformations in RSV S9 and HIV-1 proteases and in the two dimers of HIV-1 protease.

Interaction of RSV S9 Protease with the Inhibitor. Interactions with the CA-p2 inhibitor have been compared for RSV S9 and HIV-1 proteases (Figure 4). The inhibitor binding site was formed by RSV S9 protease residues from both subunits in the dimer. Residues Leu 35, Asp 37, Gly 39, Ala 40, Asp 41, Asp 42, Asn 61, Gln 63, Ile 64, His 65, Gly 66, Ile 67, Pro 105, Val 106, and Ile 108 in one subunit bind inhibitor residue P1 Leu to P4′ Nle. In the other subunit, residues Leu 35′, Asp 37′, Gly 39′, Ala 40′, Asp 41′, Gln 63′, His 65′, Gly 66′, Ile 67′, Pro 105′, and Val 106′ bind P3 Arg to P2′ Glu of the inhibitor. These residues are identical in HIV-1 protease, with the exception of Asn 61, Gln 63, and His 65 in the RSV S9 protease flaps. The side chains of Asn 61, Gln 63′, and His 65 formed hydrogen bond interactions with the inhibitor NH_2 group of P4′, the amide of P3, and the carbonyl oxygen of P4′, respectively. No equivalent side chains are present in HIV-1 protease. It was notable that the conserved set of HIV-1 protease−inhibitor hydrogen bond interactions (*22*) also occurred between the equivalent residues of RSV S9 protease and the

Table 5: Hydrogen Bond Interactions with the CA-p2 Analogue Inhibitor

inhibitor[a]		HIV-1 PR				RSV S9 PR		
				distance (Å)				
residue	atom	residue	atom	dimer 1[b]	dimer 2[b]	residue	atom	distance (Å)
P3 Arg	NH1	Met 46′	O		3.50			
	N	Asp 30′	OD2	3.45		Gln 63′	OE1	2.47
	N	Asp 29′	OD2	3.25				
	N	Gly 48′	O		3.40			
	O	Asp 29′	N	2.86	2.72	Asp 41′	N	3.18
P2 Val	N	Gly 48′	O	3.11	3.05	His 65′	O	3.09
	O	Wat[c]	O	2.97	2.84	Wat[c]	O	2.68
P1 Leu	N	Gly 27′	O	3.12	2.86	Gly 39′	O	3.37
P1′Phe	O	Wat[c]	O	2.87	2.72	Wat[c]	O	2.65
P2′Glu	N	Gly 27	O	3.09	3.23	Gly 39	O	3.00
	O	Asp 29	N	2.82	2.94	Asp 41	N	2.98
	OE1	Asp 29	N	3.02				
	OE1	Asp 30	N	2.87	2.91	Asp 42	N	3.09
	OE1	Asp 30	O	3.36[d]	3.18[d]	Asp 42	O	2.88[d]
	OE2	Asp 30	OD2	2.83[d]	3.01[d]	Asp 42	OD2	2.72[d]
P3′Ala	N	Gly 48	O	3.10	3.02	His 65	O	3.12
	O	Gly 48	N	3.48	2.97	His 65	N	3.11
P4′Nle	N	Asp 29	OD2	3.02		Asp 42	OD2	3.46
	O	Lys 45	NZ		2.80	His 65	NE2	3.13
	NH2	Met 46	O	3.40	3.29	Asn 61	OD1	3.45
	NH2				Gln 63	O	3.45	
Wat	O	Ile 50	N	2.51	2.75	Ile 67	N	3.02
		Ile 50′	N	2.84	3.03	Ile 67′	N	3.51

[a] The inhibitor is Arg-Val-Leu-r-Phe-Glu-Ala-Nle-NH_2, where r is the reduced peptide bond, $-CH_2-NH-$, and Nle is norleucine. [b] Dimers 1 and 2 comprise the asymmetric unit of the HIV-1 protease crystal. A prime indicates residues from the second subunit in each dimer. In dimer 2, the two subunits have the opposite arrangement to those of dimer 1. [c] Wat indicates the conserved water molecule. [d] Proton-mediated interactions.

inhibitor (Table 5). The main-chain atoms of the inhibitor from the carbonyl oxygen of P3 Arg to the carbonyl oxygen of P4′ Nle formed hydrogen bond interactions with the RSV S9 protease. The distribution of hydrogen bond lengths was similar for both RSV S9 and HIV-1 protease−inhibitor interactions, and the inhibitor−water hydrogen bond distances were relatively short, as noted previously for HIV-1 protease (*22*).

Our crystal structure of HIV-1 protease with the CA-p2 analogue inhibitor showed a novel proton-mediated interaction between P2′ Glu of the inhibitor and Asp 30 of the protease. The P2′ Glu is highly conserved in the HIV-1 CA-p2 cleavage site (*23*), suggesting that the interaction with Asp 30 is also conserved. The identical proton-mediated interaction was observed between Asp 42 of RSV S9 protease and P2′ Glu of the inhibitor. Interestingly, although the RSV S9 flaps had the wild-type residues and not the equivalent residues of HIV-1 protease, they formed interactions with the inhibitor similar to those seen with HIV-1 protease. His 65 of RSV protease is equivalent to Gly 48 in HIV protease, and their main-chain atoms formed identical interactions with the inhibitor. In addition, the side chain of His 65 formed a hydrogen bond interaction with the carbonyl oxygen of P4′ Nle of the inhibitor, which effectively replaced the hydrogen bond interaction of Lys 45 of HIV-1 protease.

Mutational Analysis of Flap Residues. The RSV protease flap residues 61−63 are unique to this enzyme and are accommodated as a small loop at the base of each flap. Removal of residues 61−63 was predicted to produce RSV flaps that were the same length and character as those of HIV-1 protease (*4*). Moreover, molecular modeling had predicted that these extra residues of RSV protease could potentially influence substrate binding in the S4, S4′, S3, and S3′ subsites. To test whether the loop structure was necessary for substrate hydrolysis, several mutant proteases containing deletions and/or amino acid substitutions in the region of residues 59−65 were constructed. These mutants included deletion of residues 62−63, 61−63, or 59−61 and were all catalytically inactive (results not shown). Additional mutations were made in an attempt to restore activity to these deletion mutants by substituting the structurally equivalent residues of HIV-1 protease. These constructs included deletion of 61−63 and substitutions of A59K, A60M, and H65G and deletion of 59−60 and substitutions of N61K and H65G. These mutants also were catalytically inactive. The only active protease resulted from substitution of residues 62−63 with glycines. This P62G, Q63G mutant had almost the same activity as the wild type but showed no change in specificity for a NC-PR peptide substrate with His, Glu, or Arg substituted for Pro in P4, Arg substituted for Ala in P3, Ala substituted for Val in P2, Ile substituted for Leu in P1′, or His substituted for Thr in P4′ (results not shown). Therefore, mutational analysis confirmed the importance of the flap residues 59−65 for catalysis.

DISCUSSION

The RSV S9 protease structure has significantly advanced our understanding of the molecular basis for the specificity differences of RSV and HIV proteases, since it demonstrates how RSV protease binds to a peptidic inhibitor. The residues of the flap regions, which were not visible in the original crystal structure of wild-type RSV protease (*2*), interact closely with the inhibitor. The flap residues 64−76 of RSV S9 protease have conformations similar to those of HIV-1 protease flap residues 47−59 in each subunit. Residues 65 and 67 from each subunit formed hydrogen bond interactions with the C═O and NH groups of the peptidic inhibitor similar to those conserved in numerous crystal structures of HIV

protease. The amide of Ile 67 from both flaps had the same water-mediated interaction with inhibitor that was observed for Ile 50 and 50′ in HIV protease. These interactions were predicted by our modeling studies (*4*). Differences in conformation were observed for flap residues amino-terminal to 64 compared to the equivalent region of HIV protease. Differences in amino acid sequence, length, and conformation gave rise to different interactions with the distal residues of the inhibitor in RSV S9 and HIV proteases. The side chains of His 65, Asn 61, and Gln 63 in RSV S9 protease interacted with the ends of the inhibitor, and these interactions were not possible for HIV protease due to the absence of equivalent side chains. Instead, the nonequivalent residues Lys 45 and Met 46 of HIV protease make different hydrogen bond interactions with the distal residues of the inhibitor (Figure 4 and Table 5). These different interactions were not predicted by our previous model (*4*).

Although the flap side chains differed in RSV S9 and HIV-1 proteases, the main-chain conformation of the flaps was very similar. Also, the interactions with the CA-p2 analogue inhibitor were almost identical for both RSV S9 and HIV-1 proteases, especially for inhibitor positions P2−P3′. These structural similarities explained the similar inhibition constants measured for RSV S9 and HIV-1 proteases with the CA-p2 and p2-NC analogue inhibitors (Table 2) and with KNI 272 (*7*). Both HIV-1 and RSV proteases select for larger hydrophobic residues at P1 and P1′ (*4*), such as P1 Leu and P1′ Phe in the CA-p2 analogue, despite the amino acid differences of V104/T80, R105/P81, G106/V82, and S107/N83 in the S1 and S1′ subsites of RSV and HIV-1 protease, respectively. Therefore, the 700-fold-poorer inhibition of wild-type RSV protease by the CA-p2 analogue is attributed principally to differences in the smaller S2 and S2′ subsites. However, the structural explanation is limited by the absence of any experimental structure for the flaps or inhibitor bound to this enzyme. As predicted previously from models (*6*), substitutions I42D and I44V alter the size and hydrophobicity of the S2 and S2′ subsites, while M73V and A100L have little effect on substrate specificity. RSV protease with the single substitution of the smaller Val for Ile 44 had improved activity for substrates with the larger hydrophobic Leu instead of P2 Val or P2′ Ala (*6*), while the I42D mutant had increased activity for Leu compared to P2 Val. In the crystal structure of RSV S9 protease, I42D also showed the proton-mediated interaction with P2′ Glu that was observed in HIV protease. However, in the wild-type RSV protease, the relatively large polar P2′ Glu in the CA-p2 inhibitor cannot readily bind in the smaller, more hydrophobic S2′ subsite due to the presence of the larger and nonpolar Ile instead of the smaller Val 44 and the charged Asp 42.

Differences were observed in the conformation and interactions of the distal inhibitor residues at P3 and P4′ (Figure 4). These differences did not significantly alter the measured inhibition constants, which suggested that inhibitor interactions in subsites S2−S2′ are more critical for binding than interactions in distal subsites S4−S3 and S3′−S4′. The close reproduction in RSV S9 protease of the P2−P3′ inhibitor interactions of HIV-1 protease suggested that the RSV S9 complex will be relevant for the understanding of drug binding to HIV protease. The protease inhibitors that are used as drugs to treat AIDS are all relatively small and equivalent to short peptides with various groups in the P2−P2′ or P2−P3′ positions. Therefore, the most critical interactions of RSV S9 protease with inhibitors are expected to be the same as those that are most critical for drug binding to HIV-1 protease. However, to completely reproduce the substrate specificity of HIV-1 protease will require additional changes. RSV S9 protease catalyzed hydrolysis of peptides analogous to the CA-p2 and NC-p2 inhibitors was 4- to 7-fold lower than that of HIV-1 protease. Apparently, substrate hydrolysis requires the correct protease interactions with distal substrate residues P4−P3 and P3′−P4′. Many of these interactions are mediated by flap residues, Asn 61, Gln 63, and His 65. These flap residues and other residues at the protein surface near subsites S4/S4′ and S3/S3′, such as His 7, will need to be altered in order to fully duplicate the substrate recognition of HIV-1 protease. This new crystal structure of RSV S9 protease with inhibitor will aid in future identification of the protease residues that are critical for specificity in the S4/S4′ and S3/S3′ subsites.

Previously, our published data indicated that deletion of residues 61−63 resulted in an enzyme with an increased catalytic rate (*6*). However, subsequent analysis has revealed this to be incorrect. All tested deletions in this region of the flap inactivated the enzyme. Several additional flap deletion mutants were constructed after the comparison of crystal structures in an attempt to rescue the defect introduced by the deletion. However, none of these efforts were successful, since all of these constructs were inactive. The only exception was the substitution of glycine for residues 62−63, which maintained the polypeptide backbone length of the loop region at the base of the flap. This glycine substitution resulted in a protease that was almost as active as wild type. Moreover, it did not change the specificity for NC-PR peptide substrates with single amino acid substitutions in the P4, P3, P2, P1′, or P4′ positions. Taken together, these results indicate that the residues at the base of the flap are essential for efficient binding of substrate and catalysis but may not influence substrate selection directly. Amino acid substitution of conserved flap residues 69 and 70 produced catalytically inactive enzymes (*24*). Similarly, HIV-1 protease mutants with deletions or substitution of flap residues all showed greatly reduced catalytic activity (*25*). In addition, saturation mutagenesis of the HIV-1 protease residues 46−56 indicated that these flap residues do not tolerate amino acid substitutions well (*26*). Thus, the retroviral protease flaps are very sensitive to mutations, making it difficult to identify which residues influence the substrate specificity.

Finally, several of the residues that were mutated in the RSV S9 protease are structurally equivalent to the sites of drug-resistant mutations of HIV-1 protease. The RSV protease residues I42, I44, R105, and G106 correspond to the sites of drug-resistant mutations of HIV-1 protease residues D30, V32, P81, and V82, as we predicted previously (*27*). HIV resistance to protease inhibitors arises by small changes in at least 26 mostly hydrophobic residues (*28*). Many of the resistant variants involve changes in the residues forming the substrate binding site that are expected to directly lower the affinity for the tested inhibitor. In addition, drug resistance can arise by mutation of residues outside of the substrate binding site. It is not obvious what kinetic or structural properties are altered by these resistant variants.

However, we have demonstrated success in understanding the molecular basis for the specificity differences of HIV-1 and RSV proteases by correctly reproducing the inhibitor recognition and affinity of HIV-1 protease in the engineered RSV S9 protease. The RSV S9 protease provides a model for the extent of variation that is possible without affecting inhibitor affinity. This model will be important for understanding the development of drug resistance in HIV.

ACKNOWLEDGMENT

We thank Charles Reed for help with Figure 4.

REFERENCES

1. Miller, M., Jaskólski, M., Mohana Rao, J. K., Leis, J., and Wlodawer, A. (1989) *Nature 337*, 576−579.
2. Jaskólski, M., Miller, M., Mohana Rao, J. K., Leis, J., and Wlodawer, A. (1990) *Biochemistry 29*, 5889−5898.
3. Wlodawer, A., and Erickson, J. W. (1993) *Annu. Rev. Biochem. 62*, 543−585.
4. Grinde, B., Cameron, C. E., Leis, J., Weber, I., Wlodawer, A., Burstein, H., Bizub, D., and Skalka, A.-M. (1992) *J. Biol. Chem. 267*, 9491−9498.
5. Cameron, C., Grinde, B., Jentoft, J., Leis, J., Weber, I., Copeland, T., and Wlodawer, A. (1992) *J. Biol. Chem. 267*, 23735−23741.
6. Cameron, C. E., Ridky, T. W., Shulenin, S., Leis, J., Weber, I. T., Copeland, T., Wlodawer, A., Burstein, H., Bizub-Bender, D., and Skalka, A. M. (1994) *J. Biol. Chem. 269*, 11170−11177.
7. Ridky, T. W., Bizub-Bender, D., Cameron, C., Weber, I. T., Wlodawer, A., Copeland, T., Skalka, A. M., and Leis, J. (1996) *J. Biol. Chem. 271*, 10538−10544.
8. Aiyar, A., Xiang, Y., and Leis, J. (1995) in *Methods in Molecular Biology* (Trower, M., Ed.) Vol. 57, pp 177−191, Humana Press Inc., Totoua, NJ.
9. Mildner, A. M., Rothrock, D. J., Leone, J. W., Bannow, C. A., Lull, J. M., Reardon, I. M., Sarcich, J. L., Howe, W. J., Tomich, C.-S. C., Smith, C. W., Heinrickson, R. L., and Tomasselli, A. G. (1994) *Biochemistry 33*, 9405−9413.
10. Wondrak, E. M., and Louis, J. M. (1996) *Biochemistry 35*, 12957−12962.
11. Tozser, J., Weber, I. T., Gustchina, A., Blaha, I., Copeland, T. D., Louis, J. M., and Oroszlan, S. (1992) *Biochemistry 31*, 4793−4800.
12. Dixon, M. (1953) *Biochem. J. 55*, 170−171.
13. Maibaum, J., and Rich, D. (1988) *J. Med. Chem. 31*, 625−629.
14. Bhat, T. N., Baldwin, E. T., Liu, B., Cheng, Y.-S., and Erickson, J. W. (1994) *Nat. Struct. Biol. 1*, 552−556.
15. Weber, I. T., Wu, J., Adomat, J., Harrison, R. W., Kimmel, A. R., Wondrak, E. M., and Louis, J. M. (1997) *Eur. J. Biochem. 249*, 523−530.
16. Brunger, A. T. (1992) *X-PLOR version 3.1*, Yale University Press, New Haven, CT.
17. Jones, T. A. (1985) *Methods Enzymol. 115*, 157−171.
18. Wlodawer, A., Nachman, J., Gilliland, G. L., Gallagher, W., and Woodward, C. (1987) *J. Mol. Biol. 198*, 469−480.
19. Zegers, I., Maes, D., Dao-Thi, M.-H., Poortmans, F., Palmer, R., and Wyns, L. (1994) *Protein Sci. 3*, 2322−2339.
20. Miller, M., Schneider, J., Sathyanarayana, B. K., Toth, M. V., Marshall, G. R., Clawson, L., Selk, L., Kent, S., and Wlodawer, A. (1989) *Science 246*, 1149−1152.
21. Weber, I. T. (1990) *J. Biol. Chem. 265*, 10492−10496.
22. Gustchina, A., Sansom, C., Prevost, M., Richelle, J., Wodak, S. Y., Wlodawer, A., and Weber, I. T. (1994) *Protein Eng. 7*, 309−317.
23. Barrie, K. A., Perez, E. E., Lamers, S. L., Farmerie, W. G., Dunn, B. M., Sleasman, J. W., and Goodenow, M. M. (1996) *Virology 219*, 407−416.
24. Grinde, B., Cameron, C., Weber, I., Wlodawer, A., Burstein, H., Bizub, D., Skalka, A. M., and Leis, J. (1992) *J. Biol. Chem. 267*, 9481−9490.
25. Tozser, J., Yin, F. H., Cheng, Y.-S. E., Bagossi, P., Weber, I. T., Harrison, R. W., and Oroszlan, S. (1997) *Eur. J. Biochem. 244*, 235−241.
26. Shao, W., Everitt, L., Manchester, M., Loeb, D., Hutchinson, C., III, and Swanstrom, R. (1997) *Proc. Natl. Acad. Sci. U.S.A. 94*, 2243−2248.
27. Cameron, C. E., Grinde, B., Jacques, P., Jentoft, J., Leis, J., Wlodawer, A., and Weber, I. (1993) *J. Biol. Chem. 268*, 11711−11720.
28. Schinazi, R. F., Larder, B. A., and Mellors, J. W. (1996) *Int. Antiviral News 4*, 95−107.

BI972183G